44th AIAA Aerospace Sciences Meeting and Exhibit
9 - 12 January 2006, Reno, Nevada

AIAA 2006-979

Micro and Macro Hardness Measurements, Correlations, and Contact Models

M. M. Yovanovich*
Microelectronics Heat Transfer Laboratory
Department of Mechanical Engineering
University of Waterloo, Waterloo, Ontario, Canada, N2L 3G1

Brief reviews of Brinell (Meyer) and Rockwell indenters and macrohardness tests, Berkovich, Knoop and Vickers indenters and microhardness tests, and nanoindentation tests using the Berkovich indenter are given. Vickers, Brinell and Rockwell C indentation results for Ni 200, SS 304, Zr-4, and Zr-Nb are reported and correlation equations for micro and macrohardness versus penetration depth are given. Temperature effects on yield strength, Brinell and Vickers hardness are given and correlation equations are presented to account for elevated temperatures. Models are presented for calculation of the appropriate value of contact microhardness which depends on apparent contact pressure and the effective surface roughness of the joint. Examples are given to illustrate the use of the correlation equations.

Nomenclature

A	surface area of a single tube, m^2
A_a, A_c A_V	apparent area, contact area, m^2
a	contact radius, m
B	unloading curve correlation coefficient
C_c	dimensionless contact conductance, $C_c = \sigma h_c/mk_s$
C_T	correlation coefficient, $^\circ C^{-1}$
$^\circ$C	degree Celsius
c_p, c_v	specific heats at constant pressure and volume, J/kgK
c_1	Vickers correlation coefficient, GPa
c_2	Vickers size index
D	ball diameter, mm
d	indentation diameter or diagonal, mm
d_V	Vickers diagonal, mm
E	specimen elastic modulus, GPa
E_i	indenter elastic modulus, GPa
E_r	reduced elastic modulus, $E_r^{-1} = (1-\nu^2)/E + (1-\nu_i^2)/E_i$, GPa
erfc$(\cdot)$	complementary error function
erfc$^{-1}(\cdot)$	inverse complementary error function
F	indentation load, mN
f_g	gas gap function

*Distinguished Professor Emeritus, Department of Mechanical Engineering, Fellow AIAA.

g	acceleration constant, 9.81m/s^2
H	nano, micro, macrohardness, kg/mm^2, GPa
H_B	Brinell hardness number, kg/mm^2, GPa
H_{BGM}	geometric mean of minimum and maximum Brinell hardness, kg/mm^2, GPa
H_{BK}	Berkovich hardness number, kg/mm^2, GPa
H_K	Knoop hardness number, kg/mm^2, GPa
H_M	Meyer hardness number, kg/mm^2, GPa
H_{RC}	Rockwell C hardness number
H_V	Vickers hardness number, kg/mm^2, GPa
h_c, h_g, h_r	contact, gap, radiation conductances, W/m^2 $\cdot$K
h_j	joint conductance, $h_j = h_c + h_g + h_r$, W/m^2 $\cdot$K
h	indentation depth, nm
h_f, h_{max}	final and maximum indentation depths, nm
K	absolute temperature, kelvin
I_g	gas gap integral
J	unit of energy, joule
k	thermal conductivity, W/m $\cdot$ K
k_1, k_2	solid thermal conductivities, W/m $\cdot$ K
k_g	gas thermal conductivity, W/m $\cdot$ K
k_s	effective thermal conductivity, $k_s = 2k_1k_2/(k_1 + k_2)$, W/m $\cdot$ K
M	gas gap parameter, $M = \alpha\beta\Lambda$, m
m_1, m_2, m	mean asperity slopes, effective slope, $m = \sqrt{m_1^2 + m_2^2}$
n	contact spot density, m^{-2}
P	contact pressure, GPa
P	indentation load, mN
P_a	apparent contact pressure, MPa
P_g	gas pressure, kPa
$P_{g,0}$	reference gas pressure, kPa
P_{max}	maximum indentation load, mN
Pr	Prandtl number, ν/α
Q	heat transfer rate, W
Q_j	joint heat transfer rate, W
R	thermal resistance, K/W
S_y	yield strength, GPa
S	contact stiffness, dP/dh, mN/nm
T	temperature, Celsius and absolute, °C, K
T_g	gas temperature, K
$T_{g,0}$	reference gas temperature, K
T_{rm}	room temperature, °C
T_m	melt temperature, °C
t	local gap thickness, μm
ΔT_j	joint temperature drop, K
u	dimensionless local gap thickness, t/σ
W	energy per unit time, watt
Y	mean plane separation, μm
Z	normalized Brinell hardness, $Z = H_B/H_{BGM}$

Greek Symbols

α	thermal diffusivity, m^2/s

α_1, α_2	accommodation coefficients
α	gas gap accommodation parameter, $\alpha = (2-\alpha_1)/\alpha_1 + (2-\alpha_2)/\alpha_2$
β	gas gap parameter, $\beta = 2\gamma/(\gamma+1)Pr$
γ	ratio of specific heats, c_p/c_v
ϵ	relative real contact area, $\epsilon = \sqrt{A_r/A_a}$
ϵ	factor in nanoindentation test
Λ	molecular mean free path, nm
Λ_0	reference molecular mean free path, nm
λ	relative mean plane separation, Y/σ
μ	micro
ν	Poisson's ratio
π	pi
ρ	mass density, kg/m^3
σ_1, σ_2	surface roughnesses, μm
σ	effective joint roughness $\sigma = \sqrt{\sigma_1^2 + \sigma_2^2}$, μm
σ_0	reference effective joint roughness, 1μm
ψ	thermal constriction parameter, $\psi = (1-\epsilon)^{1.5}$

Subscripts

a	apparent
B	Brinell
BK	Berkovich
b	bulk
c	contact
e	effective
g	gas, gap
i	indenter
K	Knoop
M	Meyer
m	mean, material
max	maximum
min	minimum
RC	Rockwell C
r	real
V	Vickers

I. Introduction

WHENEVER heat transfer occurs across a mechanical joint formed by two conforming rough solids there is a measurable temperature drop ΔT_j which is associated with the joint heat transfer rate Q_j. The joint temperature drop and the joint heat transfer rate are related to the joint conductance h_j and the joint thermal resistance R_j by means of the following relationships:

$$Q_j = h_j A_a \Delta T_j \qquad \text{and} \qquad Q_j = \frac{\Delta T_j}{R_j} \tag{1}$$

where A_a is the apparent area (nominal area) of the joint. The joint conductance and resistance are related:

$$R_j = \frac{1}{h_j A_a} \tag{2}$$

Thermal joint conductance h_j is a complex microgeometrical, thermal, and physical parameter which depends on the thermophysical properties of the contacting solids, the thermal properties of the substance in the microgaps, and the mechanical load applied to the joint.

The models for predicting the joint conductance are based on three separate models: (1) a microgeometric model that describes the surface roughness features of the contacting surfaces and the resultant contact, (2) the mechanical interaction of the contacting asperities, and (3) the thermal constriction/spreading resistances at the microcontacts and the heat transfer across the microgaps by conduction only or conduction and radiation when the gap substance is transparent to radiation.

There are mechanical models for conforming rough surfaces whose contacting asperities deform (i) elastically, (ii) plastically, or (iii) elastoplastically.

Several microgeometrical, mechanical and thermal models have been developed over four decades by numerous researchers for the many types of joints that occur in the microelectronics and aerospace industries. Comprehensive reviews of the various types of models are presented in Chapter 4[1] and Chapter 16[2].

This paper will be restricted to the joint formed by two conforming rough surfaces as depicted in Fig. 1. The joint of interest can be modeled as an equivalent joint formed by the contact of an equivalent rough surface and an ideal, smooth, flat surface as shown in Fig. 1.

In this paper the plastic contact model will be examined in some detail because it can be applied to many practical problems encountered in industry. The plastic contact model requires knowledge of the *microhardness* of the contacting asperities. It will be shown that this important physical parameter appears in the contact and gap components of the joint conductance.

The paper will review the different types of indentation tests using different types of indenters which result in a measure of the resistance of the material to penetration of the indenter. The resistance to penetration of the indenter is called the *hardness* of the material.

The indentation tests fall into three types of indentations: (i) macroindentations as determined by the Brinell (Meyer) and Rockwell indenters, (ii) microindentation as determined by the Berkovich, Knoop and Vickers indenters, and (iii) nanoindentation as determined by the Berkovich indenter.

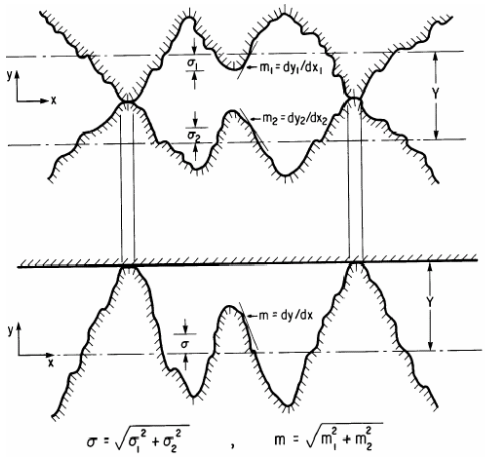

Figure 1. Typical Joints Between Conforming Rough Surfaces.

Correlation equations will be presented for the Vickers microhardness measurements as a function of the Vickers diagonal or the penetration depth. It will be shown that the Vickers microhardness correlation equations for different materials depend on two correlation coefficients which are closely related to the Brinell hardness. The correlation equations and a mechanical model will be used to predict the appropriate value for the contact microhardness given the effective joint roughness and mechanical load. The Brinell hardness and the Vickers microhardness are temperature dependent and correlation equations will be presented for three metals to illustrate this fact.

II. Contact, Gap, Radiation, and Joint Conductances

Steady heat transfer across a joint formed by the static contact of two conforming rough surfaces is given by the relationship:

$$Q_j = h_j \, A_a \, \Delta T_j \tag{3}$$

where ΔT_j is the overall temperature drop across the joint, h_j is the joint conductance, and A_a is the apparent area of the joint. If the microgaps are occupied by a gas which is transparent to radiation, then the joint conductance consists of three components such that

$$h_j = h_c + h_g + h_r \tag{4}$$

where h_c is the contact conductance, h_g is the gap conductance, and h_r is the radiation conductance. If the temperature level of the joint is below 600°C, the radiation conductance is negligibly small relative to the contact and gap conductances, and, therefore, the joint conductance is given by

$$h_j = h_c + h_g \tag{5}$$

which applies to many joints of interest to the microelectronics industry. If the joint is in an environment where the gas pressure is much smaller than one atmosphere, then the joint conductance is related to the contact conductance, and

$$h_j = h_c \tag{6}$$

This simple relation is applicable to many joints of interest to the aerospace industry when radiation is negligible[2].

The contact conductance for the joint formed by two conforming rough surfaces is given by following general relationship[1,4]:

$$h_c = \frac{2nak_s}{\psi(\epsilon)} \tag{7}$$

where n denotes the contact spot density, a is the mean contact spot radius, and the effective thermal conductivity of the joint is[1,4]

$$k_s = \frac{2k_1k_2}{k_1 + k_2} \tag{8}$$

The thermal conductivities of the contacting asperities are k_1 and k_2, respectively. The constriction/spreading resistance parameter for isothermal contact spots is[1−4]

$$\psi(\epsilon) = (1 - \epsilon)^{1.5} \tag{9}$$

where the relative contact spot size is $\epsilon = \sqrt{A_r/A_a}$ and the total real contact area is A_r.

The general relationship for the contact conductance applies to all joints formed by two conforming rough surfaces whose asperities have Gaussian height distributions with respect to mean planes associated with each surface shown in Fig. 1. The asperities are also assumed to be randomly distributed in the contact plane. The contact conductance relation was developed by Cooper, Mikic and Yovanovich[3] and its applicable to joints where the contacting asperities deform (i) elastically, (ii) plastically, or (iii) elastoplastically. The Cooper, Mikic and Yovanovich model (CMY)[3] is based on the plastic deformation of the contacting asperities. This model has been shown to be applicable to most joints when the appropriate value of the contact microhardness is used.

The CMY model consists of the following relationships for the microgeometry of the joint[1,3,4]:

$$\frac{A_r}{A_a} = \frac{1}{2}\text{erfc}\left(\frac{\lambda}{\sqrt{2}}\right) \tag{10}$$

$$n = \frac{1}{16}\left(\frac{m}{\sigma}\right)^2 \frac{\exp(-\lambda^2)}{\text{erfc}(\lambda/\sqrt{2})} \tag{11}$$

$$a = \sqrt{\frac{8}{\pi}}\left(\frac{\sigma}{m}\right)\exp\left(\frac{\lambda^2}{2}\right)\text{erfc}\left(\frac{\lambda}{\sqrt{2}}\right) \tag{12}$$

$$na = \frac{1}{4\sqrt{2\pi}}\left(\frac{m}{\sigma}\right)\exp\left(-\frac{\lambda^2}{2}\right) \tag{13}$$

The effective joint roughness parameters are defined as

$$\sigma = \sqrt{\sigma_1^2 + \sigma_2^2} \qquad\qquad m = \sqrt{m_1^2 + m_2^2} \tag{14}$$

when the surface asperities heights are Gaussian and they are randomly distributed in the plane of contact. The RMS surface roughnesses are σ_1 and σ_2. The mean asperity slopes are m_1 and m_2. The important micro-geometric parameter which appears in all relations is the relative mean plane separation which is defined as

$$\lambda = \frac{Y}{\sigma} \tag{15}$$

where Y is the mean planes separation. This parameter depends on the apparent contact pressure P and the mode of asperity deformation.

The gap conductance model for the microgaps occupied by a gas was developed by Yovanovich and co-workers[5,7,8]. Its given as an integral[1,5,7]:

$$h_g = \frac{k_g}{\sigma} \frac{1}{\sqrt{2\pi}} \int_0^\infty \frac{\exp\left[-(\lambda - u)^2/2\right]}{u + M/\sigma} du = \frac{k_g}{\sigma} I_g \tag{16}$$

where k_g is the thermal conductivity of the gas. The dimensionless local gap thickness is defined as $u = t/\sigma$. The complex gas gap rarefaction parameter is defined as[1,5,7]

$$M = \alpha\beta\Lambda \tag{17}$$

where

$$\alpha = \frac{2 - \alpha_1}{\alpha_1} + \frac{2 - \alpha_2}{\alpha_2} \tag{18}$$

$$\beta = \frac{2\gamma}{(\gamma + 1)Pr} \tag{19}$$

$$\Lambda = \Lambda_0 \left(\frac{T_g}{T_{g,0}}\right) \left(\frac{P_{g,0}}{P_g}\right) \tag{20}$$

The accommodation parameter α depends on the thermal accommodation parameters α_1, α_2 in a complex manner[1,8]. The thermal accommodation coefficients must be determined by experiments for the particular gas-solid combination[1,8].

The gas parameter β depends on the ratio of specific heats $\gamma = c_p/c_v$ and the Prandtl number Pr. The molecular mean free path Λ depends on the reference value Λ_0 and the gas temperature T_g and the gas pressure P_g, as well as the reference gas temperature $T_{g,0}$ and reference gas pressure $P_{g,0}$.

Negus and Yovanovich[7] gave the following correlation equations for the gap integral:

$$I_g = \frac{f_g}{\lambda + M/\sigma} \tag{21}$$

In the range $2 \leq \lambda \leq 4$:

$$f_g = 1.063 + 0.0471\,(4 - \lambda)^{1.68}\,[\ln(\sigma/M)]^{0.84} \quad \text{for} \quad 0.01 \leq M/\sigma \leq 1$$

$$f_g = 1 + 0.06\,(\sigma/M)^{0.8} \quad \text{for} \quad 1 \leq M/\sigma < \infty$$

The correlation equations have a maximum error of approximately 2%.

The important micro-geometric parameter λ appears in the contact and gap conductances. In general this parameter lies in the range: $2 \leq \lambda \leq 4$. When the contact pressure is light, e.g., $P \leq 0.27\,\text{MPa}$ and the contacting surfaces are hard metals, then λ will be near 4. On the other hand when the contact pressure is high, e.g., $P \geq 13.5\,\text{MPa}$, and the contacting surfaces are soft, then λ will be near 2.

To determine the value of λ its necessary to assume a mode of deformation of the contacting asperities such as plastic deformation and to apply a force balance at the joint to obtain a relationship for λ.

A force balance gives the following relationship:

$$F = PA_a = \sum_{i=1}^{N} H_{c,i} A_{r,i} \tag{22}$$

where P is the apparent contact pressure, A_a is the apparent or nominal contact area, $H_{c,i}$ is the microhardness of the ith contact spot whose real area is $A_{r,i}$, and there are N microcontacts in the apparent area. We assume that there is a mean microhardness value such that $H_{c,i} \equiv H_c$ for all contact spots; therefore,

$$\sum_{i=1}^{N} H_{c,i} A_{r,i} = H_c \sum_{i=1}^{N} A_{r,i} = H_c A_r \tag{23}$$

where A_r is the total real contact area. From the force balance and the geometric relation A_r/A_a for interaction of two Gaussian surfaces, we have

$$\frac{P}{H_c} = \frac{A_r}{A_a} = \frac{1}{2}\text{erfc}\left(\frac{\lambda}{\sqrt{2}}\right) \tag{24}$$

From the foregoing relation we can write

$$\lambda = \sqrt{2}\,\text{erfc}^{-1}\left(\frac{2P}{H_c}\right) \tag{25}$$

This important relationship will be used to obtain relationships for the dimensionless contact conductance which is defined as

$$C_c = \frac{\sigma}{m}\frac{h_c}{k_s} = f(\lambda) = \frac{1}{4\sqrt{2\pi}} \frac{\exp(-\lambda^2/2)}{\left[1 - \sqrt{\frac{1}{2}\text{erfc}(\lambda/\sqrt{2})}\right]^{1.5}} \tag{26}$$

The relationships for C_c and λ were combined and a numerical method were used to obtain numerical values of C_c for values of P/H_c. The following simple power-law relation was recommended by Yovanovich[4]:

$$C_c = 1.25\left(\frac{P}{H_c}\right)^{0.95} \tag{27}$$

This explicit relationship agrees with the theoretical values to within $\pm 1.5\%$ in the range $2 \leq \lambda \leq 4.75$ and in the range $10^{-6} \leq P/H_c \leq 2.3 \times 10^{-2}$. Numerical quadrature is required to find values of λ for given values of P and H_c. The following approximations can be used to calculate λ:

Yovanovich Approximation (1981)

$$\lambda = 1.184\left[-\ln\left(3.132\,\frac{P}{H_c}\right)\right]^{0.547}$$

Song-Yovanovich Approximation (1988)

$$\lambda = 1.363\left[-\ln\left(5.589\,\frac{P}{H_c}\right)\right]^{0.5}$$

Ranges of application of the approximations are

$$2 \le \lambda \le 4.75 \qquad \text{and} \qquad 10^{-6} \le \frac{P}{H_c} \le 2 \times 10^{-2}$$

Antonetti Power-Law Approximation (1983)

$$\lambda = 1.53 \left(\frac{P}{H_c} \right)^{-0.097}$$

can be used to obtain values quickly; however, its less accurate than the other two approximations. It shows more clearly than the other approximations that λ is a relatively weak function of the relative contact pressure P/H_c.

The foregoing short reviews of the contact and gap conductances for joints formed by the mechanical contact of conforming rough surfaces show that the dimensionless parameter P/H_c is very important. Since the apparent contact P is known, it is necessary to obtain values of the contact microhardness H_c for a given joint having the effective surface roughness σ/m.

A. Iterative Model for Calculation of Contact Microhardness

The iterative model for calculating the contact microhardness H_c and the relative contact pressure P/H_c is based on a set of equations and the given joint parameters: $(\sigma/m, c_1, c_2, P, H_b)$.

The set of equations are[1,4,6]:

$$\left.\begin{array}{lrcl} (i) & \lambda & = & \sqrt{2}\,\mathrm{erfc}^{-1}\left(\dfrac{2P}{H_c}\right) \\ (ii) & a & = & \left(\dfrac{\sigma}{m}\right)\sqrt{\dfrac{8}{\pi}}\exp\left(\dfrac{\lambda^2}{2}\right)\mathrm{erfc}\left(\dfrac{\lambda}{\sqrt{2}}\right) \\ (iii) & d_V & = & \sqrt{2\pi}\,a \\ (iv) & H_c & = & c_1\left(\dfrac{d_V}{d_0}\right)^{c_2} \end{array}\right\} \tag{28}$$

The parameter $d_0 = 1\,\mu$m is introduced for convenience. The set of equations is based on the area equivalence of the Vickers projected area and the contact spot area, therefore, $A_V = d_V^2/2 = A_c = \pi a^2$. Also we assume that $H_c = H_V$.

The iteration process begins with an initial guess for H_c. It has been demonstrated that when the initial guess is based on the known bulk hardness, i.e., $H_c = H_b$, convergence occurs after 2 to 3 iterations depending on the convergence criterion[6].

To avoid the numerical calculation of the inverse complementary error function in the first equation, the approximation of Yovanovich[4] was used to calculate the inverse complementary error function.

B. Explicit Relationship for Relative Contact Pressure

Song[8] and Song and Yovanovich[9] examined the iterative model and found that when the Song and Yovanovich approximation for $\mathrm{erfc}^{-1}(\cdot)$ is used, the iterative process leads to the following explicit relationship:

$$\frac{P}{H_c} = \left[\frac{P}{1.62 c_1 \left(\sigma/\sigma_0 m\right)^{c_2}} \right]^{1/(1+0.071 c_2)} \tag{29}$$

where $\sigma_0 = 1\mu$m. This relationship shows how the important parameter P/H_c depends on the joint parameters $(\sigma/m, c_1, c_2, P)$.

In the subsequent sections it will be shown how the contact hardness can be calculated and how it is related to the macro, micro and nano-hardness. However, before this can be done its important to present brief reviews of hardness indenters and hardness tests.

III. Micro and Macro Hardness Indenters

The several micro and macrohardness indenters will be reviewed in this section.

The macrohardness indentation testers are the Brinell (Meyer) and Rockwell, and the microhardness indenters are the Berkovich, Knoop and Vickers.

There are 6 types of hardness indentation tests used to determine the macrohardness and microhardness of materials such a metals, ceramics, and plastics. The indenters are much harder than the specimen, and they are smooth balls, cones with hemispherical tips, and pyramidal having three or four faces.

A brief description of the various types of indenters are given below. More details regarding the nano, micro, and macro-indenters can be found in the texts[10–14].

A. Brinell and Meyer Macrohardness

The Brinell and Meyer macrohardness are determine by the same indentation test. A hard smooth ball of diameter D(mm) is pressed into a smooth flat surface under a known load F(N) for duration of 30 to 60 seconds depending on the whether the metal is hard or soft as shown in Fig. 2. After removal of the ball, the diameter of the indentation is measured by means of an optical microscope. The diameter of the indentation d(mm) is the average value of 2 measurements, i.e., $d = (d_1 + d_2)/2$ where d_1 and d_2 are the measured diameters which are perpendicular to each other.

Brinell Hardness Number. The Brinell hardness number (BHN) is expressed as the load divided by the *actual* area of the indentation. Therefore,

$$\text{BHN} = \frac{2F}{\pi D\left(D - \sqrt{D^2 - d^2}\right)} = \frac{F}{\pi D t} \tag{30}$$

where the penetration depth, defined as the distance from the original surface to the maximum indentation depth, is

$$t = \frac{D - \sqrt{D^2 - d^2}}{2} \tag{31}$$

The relative indentation size is recommended to lie in the range: $d/D = 0.25 - 0.6$. If the load is given in kgf and the indentation diameter is given in mm, then the Brinell hardness has units of kgf/mm^2. These are the units used in handbooks and older texts. Today, its more common to give the Brinell hardness in units of MPa or GPa. In this paper the Brinell hardness will be denoted as H_B.

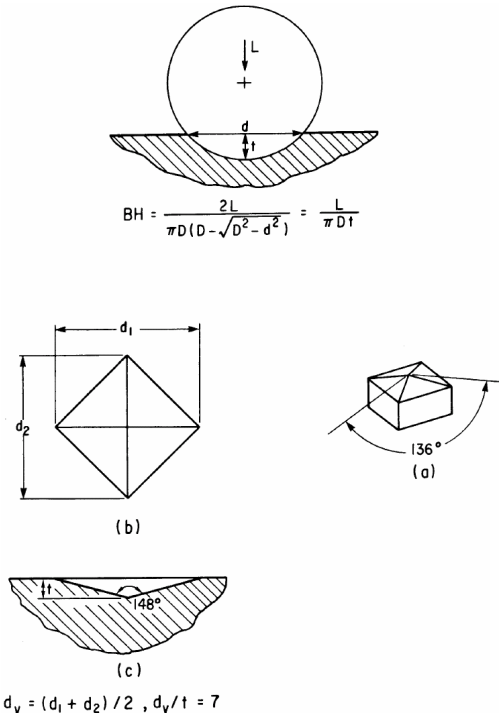

Figure 2. Brinell and Vickers Indenters and Indentations.

Meyer Hardness Number. The Meyer hardness number (MHN) is based on the same indentation test, however, the Meyer hardness number is expressed as the indentation load divided by the *projected* area of the indentation. Therefore,

$$\text{MHN} = \frac{4F}{\pi d^2} = P_m \tag{32}$$

where P_m is the mean contact pressure. The Meyer hardness is said to be a true representation of the hardness of the material. In this paper the Meyer hardness will be denoted as H_M.

The Brinell and Meyer hardness are related as

$$\frac{H_B}{H_M} = \frac{(d/D)^2}{2\left[1 - \sqrt{1 - (d/D)^2)}\right]} \tag{33}$$

Table 1 shows the relationship between the numerical values of the Brinell and Meyer hardnesses for typical values of d/D which is sometimes called the contact strain.

The difference between the Brinell hardness and the Meyer hardness is about 10% at the largest recommended value of d/D.

The Brinell hardness number is favored by certain engineers because there is an empirical relationship between it and the ultimate tensile strength of the material. The Meyer hardness which is based on the projected area is preferable since it gives the mean pressure beneath the indenter which opposes the applied force.

B. Rockwell Macrohardness

The Rockwell hardness test is a static indentation test similar to the Brinell indentation test. It differs in that it measures the permanent increase in the indentation depth from the depth reached under an initial load of 98.1 N, due to the application of an additional load. Measurement is made after recovery which takes place following the removal of the additional load. The Rockwell hardness number is a direct reading (in units of 0.002 mm) from the dial gauge which is attached to the Rockwell machine while the initial minor load is still imposed.

According to the material being tested, the indenter may be a 120° diamond cone with a blended spherical apex of 0.2 mm radius or a steel ball indenter. The steel ball indenter is normally 1.588 mm in diameter, however, larger diameters such as 3.175, 6.350, or 12.7 mm may be used for soft materials.

The Rockwell hardness testers are constructed to apply a fixed minor load of 98.1 N which is used to establish the measurement datum. This is followed by an additional load, within 2-8 seconds, which may be 0.49, 0.88 or 1.37 kN. The combination of three loads and five indenters gives fifteen conditions of test; each has its own hardness scale.

There is no Rockwell hardness number value designated by a number alone because it is necessary to specify which indenter and load have been used in an indentation test. Therefore, a prefix letter is employed to designate the scale and test condition. Of the several scales available, the B and C scales are the most widely used. For the B scale, a 0.88 kN additional load with a 1.588 mm diameter steel ball indenter is used. For the C scale, a 1.37 kN additional load a conical indenter is used.

The Rockwell scales are divided into 100 divisions, each equivalent to 0.002 mm of recovered indentation. Since the scales are reversed, the number is higher the harder the material, as shown by the following relations which define the Rockwell B and C hardness numbers.

Table 1. Ratio of Brinell to Meyer hardness versus contact strain

d/D	H_B/H_M
0.20	0.9899
0.30	0.9770
0.40	0.9583
0.50	0.9330
0.60	0.9000

$$\left.\begin{aligned} \text{Rockwell B} &= \text{RB} = 130 - \frac{\text{depth of penetration (mm)}}{0.002} \\ \text{Rockwell C} &= \text{RC} = 130 - \frac{\text{depth of penetration (mm)}}{0.002} \end{aligned}\right\} \tag{34}$$

The Brinell (Meyer) hardness tests and the Rockwell tests give essentially identical macrohardness values which are constant with respect to the indentation load. The hardness values correspond to the resistance of the bulk material to the penetration of the indenter. Brinell hardness values are frequently reported in materials handbooks.

C. Knoop Microhardness Indenter and Test

The Knoop (HK) hardness indenter and test procedure was developed at the National Bureau of Standards (now NIST) in 1939. The indenter used is a rhombic-based pyramidal diamond that produces an elongated diamond shaped indent. The angles from the opposite faces of a Knoop indenter are $172°30'$ and $130°$.

The Knoop indenter is a diamond ground to pyramidal form that produces a diamond shaped indentation having approximate ratio between long and short diagonals of 7 to 1. The depth of indentation is about 1/30 of the diagonal length.

The Knoop indenter is particularly useful for the study of highly brittle materials due to the small depth of penetration for a given indenter load. Also, due to the unequal lengths of the diagonals, it is very useful for investigating anisotropy of the surface of the specimen.

Knoop tests are mainly done at test forces from 10g to 1000g, so a high powered microscope is necessary to measure the indent size. Because of this, Knoop tests have mainly been known as microhardness tests. The newer standards more accurately use the term microindentation tests. The magnifications required to measure Knoop indents dictate a highly polished test surface. To achieve this surface, the samples are normally mounted and metallurgically polished, therefore Knoop is almost always a destructive test.

The indenter is pressed into the polished surface of a sample by an accurately controlled test force which is maintained for a specific dwell time, normally 10 - 15 seconds. After the dwell time is complete, the indenter is removed leaving an elongated diamond shaped indent in the sample. The size of the indent is determined optically by measuring the longest diagonal d of the diamond shaped indent. The length of the smaller diagonal is $d/7$. The Knoop hardness number KHN is defined as the ratio of the test force divided by the *projected* area of the indent. The Knoop hardness number is calculated from:

$$\text{KHN} = \frac{2F}{d^2\left[\cot\frac{172.5°}{2}\tan\frac{130°}{2}\right]} = 14.240\frac{F}{d^2} \tag{35}$$

where the units of d are mm and the load is kgf. The Knoop microhardness will be denoted as H_K. The conventional units are kgf/mm^2. Typical values of H_K are in the range from 100 to 1000 kgf/mm^2. Table 2 lists nominal values for 4 materials.

Table 2. Values of Knoop hardness number for selected materials

Material	H_K
Gold foil	69
Quartz	820
Silicon carbide	2480
Diamond	8000

D. Vickers Microhardness Indenter and Test

In the Vickers microhardness test, a diamond indenter, in the form of a square-based pyramid with an angle of 136° between the opposite faces at the vertex, is pressed into the polished surface of the test specimen using a prescribed force F as shown in Fig. 2. After the force has been removed, the diagonal lengths of the indentation d_1 and d_2 are measured with an optical microscope. The time for the initial application of the force is 2 to 8 seconds, and the test force is maintained for 10 to 15 seconds. The applied loads vary from 1 to 120 kgf, and the standard loads are $5, 10, 20, 30, 50, 100$, and $120\,\text{kgf}$

The Vickers hardness number VHN is defined as the test force divided by the *actual* area of the residual indent. Its given by

$$\text{VHN} = \frac{2F}{d^2}\sin\frac{136^\circ}{2} = 1.854\frac{F}{d^2} \tag{36}$$

where the mean diagonal is $d = (d_1 + d_2)/2$ and its units are mm. The unit of load is kgf. The Vickers hardness number is smaller than the mean contact pressure by about 7%.

The Vickers microhardness will be denoted as H_V. The units of Vickers microhardness are frequently reported as kgf/mm^2. There is now a trend towards reporting Vickers microhardness in SI units (MPa or GPa). To convert Vickers microhardness values from kgf/mm^2 to MPa multiply by 9.807.

The Vickers microhardness depends on the load applied to the indenter. As the load increases, the diagonal and corresponding penetration depth increase. The Vickers microhardness can be related to the diagonal d_V or the penetration depth t which are related as $d_V = 7t$. The Vickers contact area and the penetration depth are related as $A_V = 24.5\,t^2$.

The Vickers microhardness test is reliable for measuring the microhardness of metals, polymers, and ceramics.

E. Berkovich Micro and Nanohardness Indenter and Nanohardness Tests

The Berkovich diamond indenter is a triangular pyramid with a true point since only three sides have to meet. The angle between the vertical axis and each of the faces is 65°. The Berkovich diamonds are cut with an angle of 142° between any two of the planes along the line so that the surface areas of indents are the same as the Vickers indent for the same depth of penetration. This means that isotropic microhardness values are the same for a given material when its indented by the Berkovich and the Vickers indenters.

The Berkovich indenter is used to study the micro and submicron indentations of various materials. Equipment for this purpose consists of an instrumented loading device that records the indenter load P in mN and indenter displacements h in micrometers or nanometers. Estimates of the elastic modulus E and microhardness H of the specimen are obtained from the load versus penetration measurements.

Rather than the direct measurements of the size of residual impressions, which require optical microscopes, contact areas are calculated from the depth measurements together with a knowledge of the indenter shape. This is in contrast to the procedures employed for the macro indentation tests, where the lateral dimensions (diagonals for the Vickers and Knoop tests, and diameter for the Brinell and Rockwell tests), rather than the depth of penetration of the residual impression are used to calculate the microhardness and the macrohardness.

IV. Micro and Macrohardness Tests and Correlations

The Vickers, Brinell and Rockwell B micro and macrohardness test results and correlation equations for SS 304, Ni 200, Zr-4, and Zr-Nb will be presented in this section. The data are given in several papers[6,15–17] and the dissertation of Hegazy[19]. Figures 3 and 4 show the Vickers, Brinell and Rockwell B results for SS 304 and Ni 200 respectively. In order to show the micro and macrohardness values on the same plot, its necessary to plot hardness versus the penetration depth t which varies from about $t = 1\,\mu\text{m}$ to approximately $t = 800\,\mu\text{m}$. The largest penetration depths of about $800\,\mu\text{m}$ correspond to the Brinell tests which were based

on a 10 mm diameter steel ball forced into the surface of the specimens under a 29.43 kN load. In the Rockwell B tests a 1.59 mm diameter steel ball was forced into the surface of the specimens under a 981 N load. The penetration depths were about 100 μm.

The Brinell and Rockwell B macrohardness values denoted as H_b for SS 304 were identical, $H_b = 150\,\mathrm{kg/mm^2}$ (Fig. 3). The Brinell and Rockwell B macrohardness values for Ni 200 were identical, $H_b = 170\,\mathrm{kg/mm^2}$ (Fig. 4).

The Vickers microhardness values H for both metals are dependent on the penetration depth t as shown in Figs. 3 and 4. The points shown in Fig. 3 represent the average value of 5 test values at each load.

The maximum values $H = H_{max}$ were measured at the minimum depths $t = t_0$, and the smallest values $H = H_{min}$ were measured at the maximum test depths $t = t_n$. The Vickers microhardness values were correlated and the extrapolated curve intersected the bulk values H_b at the penetration depth t_b. The Vickers microhardness values were correlated with the following general set of equations[6,15–17]:

$$\left.\begin{array}{lcll} H & = & H_{max} = \text{constant} & t \le t_0 \\ H & = & H(t) = c_1 t^{c_2} + c_3 & t_0 \le t \le t_n \\ H & = & H_b = \text{constant} & t \ge t_b \end{array}\right\} \qquad (37)$$

The correlation coefficients are c_1, c_2 and c_3. The values for SS 304 are

$$c_1 = 3049.6 \qquad c_2 = -0.024 \qquad c_3 = -2649.8 \qquad (38)$$

The maximum and minimum hardness values and the corresponding penetration depths are[6,15–17]

$$\left.\begin{array}{lcllcl} H_{max} & = & 385\,\mathrm{kg/mm^2} & t_0 & = & 1.2\,\mu\mathrm{m} \\ H_b & = & 150\,\mathrm{kg/mm^2} & t_b & = & 34\,\mu\mathrm{m} \end{array}\right\} \qquad (39)$$

The values for Ni 200 are

$$c_1 = 377.27 \qquad c_2 = -0.274 \qquad c_3 = 7.79 \qquad (40)$$

The maximum and minimum hardness values and the corresponding penetration depths are

$$\left.\begin{array}{lcllcl} H_{max} & = & 362.3\,\mathrm{kg/mm^2} & t_0 & = & 1.24\,\mu\mathrm{m} \\ H_b & = & 170.4\,\mathrm{kg/mm^2} & t_b & = & 21.56\,\mu\mathrm{m} \end{array}\right\} \qquad (41)$$

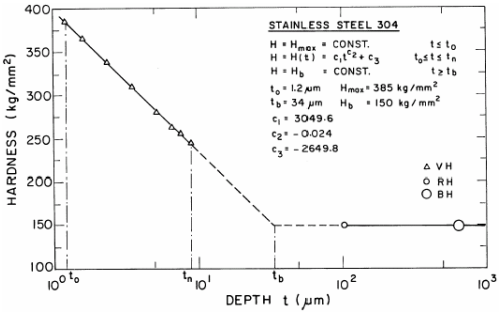

Figure 3. Vickers, Brinell, Rockwell Hardness Versus Indentation Depths for SS 304.

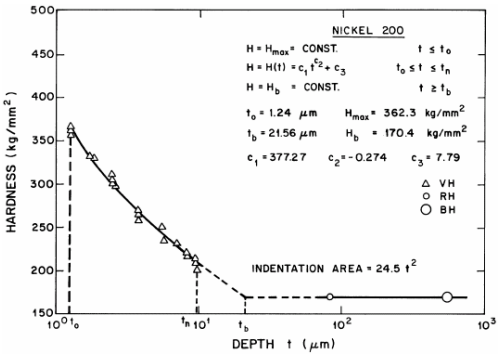

Figure 4. Vickers, Brinell, Rockwell Hardness Versus Indentation Depths for Ni 200.

In order to implement the correlation equations its necessary to convert the penetration depths to microns from μm. For example, if the Vickers penetration depth is 5×10^{-6} m for both metals, then $t = 5 \times 10^{-6}/10^{-6} = 5$ micron, and the microhardness values are $H = 284.3\,\mathrm{kg/mm^2}$ for SS 304 and $H = 250.5\,\mathrm{kg/mm^2}$ for Ni 200.

A model is required to calculate the contact microhardness given the correlation equation and the effective surface roughness σ/m and the apparent contact pressure P. Several models were presented[6,15–17]. A simple direct method for calculation of the effective contact microhardness will be presented next.

A. Direct Approximate Method

The Direct Approximate Method (DAM) is based on the observation that the geometric parameters of the CMY model change slowly as the apparent contact pressure is varied over a wide range. This model is based on the equivalence of the Vickers indentation area $A_V = d_V^2/2 = 49t^2/2$ and the mean contact spot area $A_c = \pi a^2$ where a is the mean contact spot radius. The area equivalence leads to the following relationship between the indentation depth and the contact spot radius:

$$t = \left(\frac{\pi a^2}{24.5}\right)^{1/2} = 0.358\,a \tag{42}$$

The contact microhardness can be related to the mean contact spot radius as

$$H_c = c_1\,(0.358\,a)^{c_2} + c_3 \tag{43}$$

It was shown by Yovanovich[4] that the following simple explicit relationship:

$$a = 0.99\left(\frac{\sigma}{m}\right)\left[-\ln\left(3.132\,\frac{P}{H}\right)\right]^{-0.547} \tag{44}$$

can be used to calculate the mean contact spot radius when σ/m, P and H are known.

For a particular metal such as Ni 200 we have after substitution the implicit relationship:

$$H = 501.3\left(\frac{m}{\sigma}\right)^{0.274}\left[-\ln\left(3.132\,\frac{P}{H}\right)\right]^{0.150} \tag{45}$$

where the units of σ/m must be microns, and the units of P and H must be consistent. Since the unknown H appears on both sides, a numerical method to find its root can be used, or an iterative approach can be employed to calculate the value of H beginning with an initial guess. Its found that starting with the lowest value $H = H_b$, only 2 to 3 iterations are required to calculate an accurate value of H.

The following explicit relationship based on $H = H_b$ substituted on the right hand side gives approximate values for the effective contact microhardness which is denoted as H_c:

$$H_c = 501.3\left(\frac{m}{\sigma}\right)^{0.274}\left[-\ln\left(3.132\,\frac{P}{H_b}\right)\right]^{0.150} \tag{46}$$

This relationship shows clearly how the contact microhardness is related to the effective surface roughness of the joint, the apparent contact pressure, and the bulk hardness.

For a given metal the contact microhardness decreases with increasing surface roughness and increasing contact pressure.

Two examples will be given to illustrate the use of the correlation equation. For a Ni 200 joint where $\sigma/m = 1.21/0.139 = 8.71$ microns, $P_{min} = 622\,\mathrm{kg/mm^2}$, $P_{max} = 3,510\,\mathrm{kg/mm^2}$, and $H_b = 170.4\,\mathrm{kg/mm^2}$. The mean contact pressure is $P_m = (P_{min} + P_{max})/2 = 2,066\,\mathrm{kg/mm^2}$.

Substitution of these values in the correlation equation gives the contact microhardness value: $H_c = 366.0\,\mathrm{kg/mm^2}$ which is 2.15 times greater than the bulk hardness.

For the second example the contact parameters are $\sigma/m = 8.48/0.344 = 24.65$ microns, $P_{min} = 571\,\mathrm{kg/mm^2}$, $P_{max} = 3,433\,\mathrm{kg/mm^2}$, and $H_b = 170.4\,\mathrm{kg/mm^2}$. The mean contact pressure is $P_m = (P_{min} + P_{max})/2 = 2,002\,\mathrm{kg/mm^2}$.

Substitution of these values in the correlation equation gives the contact microhardness value: $H_c = 277.3\,\mathrm{kg/mm^2}$ which is 1.63 times greater than the bulk hardness.

B. Vickers Microhardness Correlation Equations

The material in this section are obtained from the work of Hegazy[19]. The development of Vickers microhardness correlation equations are based on Vickers microhardness and Brinell hardness measurements. Seven loads from 0.147 N to 4.9 N were used in the Vickers microhardness measurements. For each load 5 indentations were used to calculate the value of H_V. Each value of H_V is based on the average of the measured diagonals for a particular load, i.e.,

$$H_V = \frac{1.854\,F}{d_V^2} \qquad \text{GPa} \tag{47}$$

where the applied load is F in newtons, and

$$d_V = \frac{(d_1 + d_2)}{2} \tag{48}$$

and d_1 and d_2 are the measured diagonals in μm.

For any load the maximum percent difference in the calculated values of H_V was less than 5 %. The Vickers microhardness values H_V in GPa for 4 metals: Ni 200, SS 304, Zr-4 and Zr-Nb are plotted against the average values of the Vickers indentation diagonal d_V in μm as shown in Figs. 5 and 6.

The Vickers microhardness values are correlated by the power-law relation:

$$H_V = c_1 \left(\frac{d_V}{d_0}\right)^{c_2} \qquad \text{with} \quad d_0 = 1\,\mu\mathrm{m} \tag{49}$$

The parameter d_0 was introduced to make the ratio d_V/d_0 dimensionless. The Vickers microhardness correlation coefficients are c_1 and c_2. The units of H_V and c_1 are GPa, and the size index c_2 is dimensionless. The correlation equation is based on the average Vickers diagonal d_V. The correlation coefficient c_1 is the Vickers microhardness when $d_V = d_0$.

The bulk or material hardness which is denoted as H_m was determined by Brinell and Rockwell B indentation tests which gave the same value although the indentations depths are significantly different as seen in Fig. 5.

The values of H_m, c_1 and c_2 are given in Table 2 for the four metals.

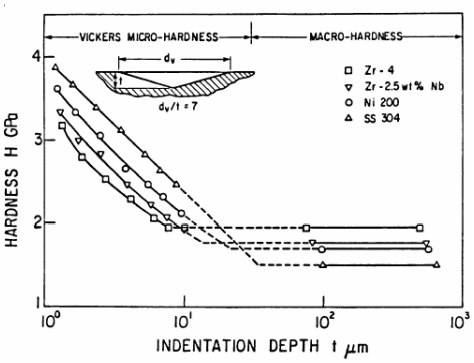

Figure 5. Vickers, Brinell, Rockwell Hardness Versus Indentation Depths for Four Metals and Alloys (From Hegazy, 1985).

The maximum and RMS percent differences between the measured values and the predicted values are given. Except for the maximum percent difference of 10.2 % for Zr-Nb, the maximum percent differences are below 5 %, and the RMS percent differences are below 3 %.

The average value of c_2 is -0.260. Since the variation in the values of c_2 is relatively small, this value was selected for the 4 metals to develop an alternative Vickers microhardness correlation equation of the form:

$$H_V = \xi \left(\frac{d_V}{d_0}\right)^{\eta} \qquad \text{with} \quad d_0 = 1\,\mu\mathrm{m} \tag{50}$$

where $\eta = -0.260$, fixed for all metals. The Vickers microhardness values were used to find values for the correlation coefficients ξ. These values are given in Table 4.

Table 3. Vickers correlation coefficients for four metals

Metal	H_m(GPa)	c_1(GPa)	c_2	Max % Diff.	RMS % Diff.
Ni 200	1.668	6.304	−0.264	4.8	1.8
SS 304	1.472	6.271	−0.229	4.2	1.4
Zr-4	1.913	5.677	−0.278	3.4	1.7
Zr-Nb	1.727	5.884	−0.267	10.2	2.7

The alternative correlation equation with the fixed value of $\eta = -0.260$ and the corresponding values of ξ have maximum and RMS percent differences which are comparable with the original correlation equation. All values of H_V/ξ when plotted against d_V fall on a single curve as seen in Fig. 7.

This confirms that there is a close relationship between H_V and ξ for the 4 metals. The values of ξ when plotted against values of H_m fall on a straight line as shown in Fig. 8. The following correlation equation for ξ versus H_m is obtained

$$\xi = 12.04 - 3.49\, H_m \qquad \text{for} \quad 1.472 \le H_m \le 1.913 \qquad (51)$$

The units of ξ and H_m are GPa. The comparisons between the actual and predicted values of ξ are given in Table 4.

The RMS percent difference is about 2.3 %.

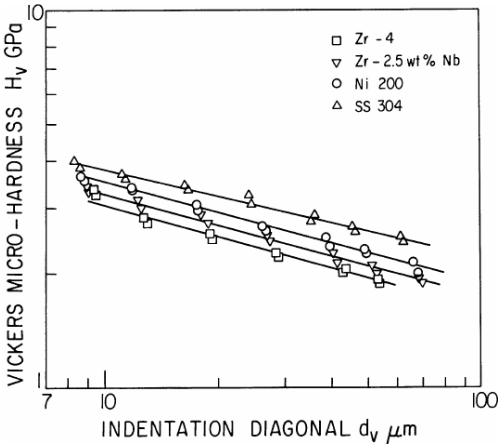

Figure 6. Vickers Hardness Versus Indentation Depths for Four Metals and Alloys (From Hegazy, 1985).

A new general Vickers microhardness correlation equation for the 4 metals and any other metal whose bulk hardness lies in the range: $1.472 \le H_m \le 1.913$ is

$$H_V = (12.04 - 3.49\, H_m) \left(\frac{d_V}{d_0}\right)^{-0.260} \qquad \text{GPa} \qquad (52)$$

where the units of H_m must be GPa.

V. Correlation Equations for Vickers Coefficients

Table 4. Modified Vickers correlation coefficients for four metals

Metal	H_m(GPa)	ξ(GPa)	η	Max % Diff.	RMS % Diff.
Ni 200	1.668	6.217	−0.260	5.2	1.8
SS 304	1.472	6.906	−0.260	5.9	2.4
Zr-4	1.913	5.367	−0.260	3.9	1.8
Zr-Nb	1.727	5.750	−0.260	9.7	2.7

Table 5. Comparisons of modified correlations with Vickers hardness values

Metal	H_m(GPa)	ξ(GPa)	Corr. Eq.	% Diff.
Ni 200	1.668	6.217	6.219	0.03
SS 304	1.472	6.906	6.903	−0.04
Zr-4	1.913	5.367	5.364	−0.06
Zr-Nb	1.727	5.750	6.013	4.60

When Vickers indentation tests were done on harder metals and alloys, it was observed that the simple general correlation equation developed for the 4 metals whose bulk hardness values lie in the range: $(1.33 \leq H_m \leq 1.91)$ GPa predicts values of H_V which have large errors.

When a Titanium alloy with $H_B = 3.07$ GPa, and untreated and heat treated tool steel with Brinell hardness values in the range: $(1.98 \leq H_B \leq 7.57)$ GPa, the simple general correlation equation gives poor agreement with the measured Vickers microhardness measurements. Sridhar[21] conducted extensive Vickers microhardness tests, and Brinell and Rockwell C macrohardness tests, and he found new relationships between the Vickers correlation coefficients c_1 and c_2 and the bulk hardness H_B. The development of the new correlation equations are given in[21,23]; only the final results will be presented.

For Brinell hardness values in the range $1.30 - 7.60$ GPa, a least-squares cubic fit was used to obtain correlation equations for c_1 and c_2. The correlation equation for c_1 is[21,23]

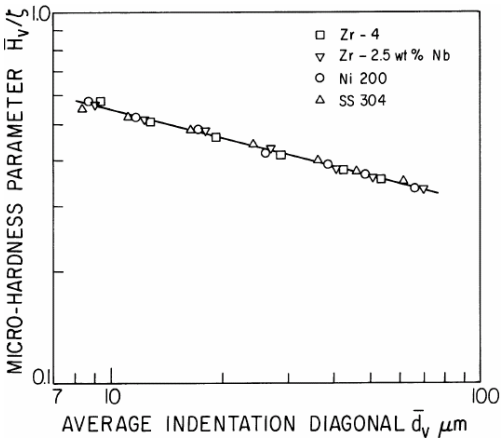

Figure 7. Normalized Vickers Microhardness Versus Vickers Diagonals four Four Metals and Alloys. (From Hegazy, 1985)

$$\frac{c_1}{H_{BGM}} = 4.0 - 5.77\,Z + 4.0\,Z^2 - 0.61\,Z^3 \tag{53}$$

with

$$Z = \frac{H_B}{H_{BGM}}$$

where $H_{BGM} = 3.178$ GPa which is the geometric mean of the minimum and maximum values of H_B for the test materials.

The correlation equation for c_2 is[21,23]

$$c_2 = -0.57 + \frac{Z}{1.22} - \frac{Z^2}{2.42} + \frac{Z^3}{16.58} \tag{54}$$

The maximum percent difference and RMS % difference between the c_1 values and the correlation equation are −11.0% and 5.3% respectively. The maximum percent difference and RMS % difference between the c_2 values and correlation equation are −41.5% and 20.8% respectively. The relatively large percent differences between the c_2 values and the correlation values are less important than the good agreement between the c_1 values and the correlation equation. The values of c_2 for the very hard heat treated tool steel lie in the range: $[-0.040$ to $-0.129]$.

An alternative correlation equation for c_2 was given[21,23]:

$$c_2 = -0.370 + 0.442\,\frac{H_B}{c_1} \tag{55}$$

The percent difference and RMS percent difference between all data and the correlation equation are 25.8% and 10.9% respectively.

The Brinell hardness tests were performed with a standard steel ball for materials with hardness less than 4.40 GPa and with a carbide ball with hardness greater than 4.40 GPa as recommended by ASTM E10. A load of 3000 kgf was used to make Brinell hardness tests so that included the entire range $(1.30 - 7.60)$ GPa

Rockwell C hardness tests were also performed on the heat treated tool steel specimens to complement the Brinell hardness tests. The Brinell hardness values and the Rockwell C hardness values in the range $(15 \leq \text{HRC} \leq 65)$ were in good agreement. The following correlation equation between the Brinell hardness number and the Rockwell C hardness number was obtained using a 3rd order polynomial:

$$\text{BHN} = 43.7 + 10.92\,\text{HRC} - \frac{(\text{HRC})^2}{5.18} + \frac{(\text{HRC})^3}{340.26} \tag{56}$$

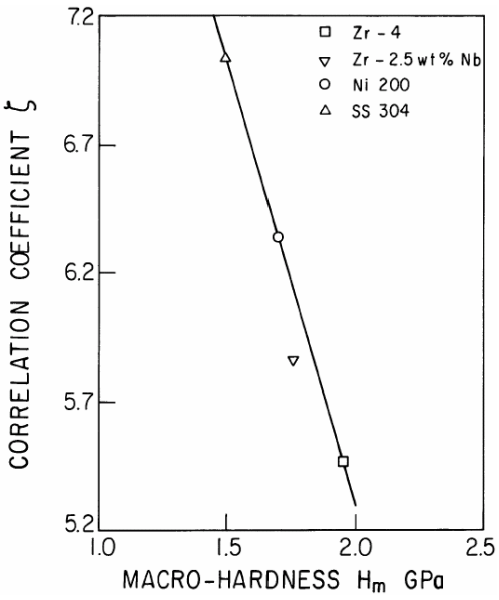

Figure 8. Plot of Vickers Coefficients Versus Macrohardness. (From Hegazy, 1985).

which is valid for $(20 \leq \text{HRC} \leq 65)$. This correlation equation is a useful relationship between Brinell hardness number (BHN) and Rockwell C hardness number (HRC) for tool steel (01). Its not possible to perform accurate Rockwell C hardness tests below HRC = 20.

VI. Temperature Effects on Vickers and Brinell Hardness

Thermophysical properties of all materials depend on temperature level. Since the temperature level of most joints is above room temperature, its important to conduct Vickers microhardness and Brinell hardness test at elevated temperatures.

A. Temperature Effects on Yield Strength and Vickers Microhardness of SS 304L

The effects of temperature level on the values of yield strength S_y and Vickers microhardness H_V are given[20] in Table 6.

Table 6. Temperature effects on yield strength and Vickers hardness

T(°C)	S_y(MPa)	$S_y(T)/S_y(25)$	H_V(MPa)	$H_V(T)/H_V(25)$
25	274	1.00	1570	1.00
200	223	0.81	1180	0.75
400	198	0.72	1090	0.69
600	157	0.57	863	0.55
800	78.9	0.29	392	0.25

The values of yield strength and Vickers microhardness are strongly dependent on temperature for temperatures from (200 to 800)°C. The temperature dependence of S_y and H_V with temperature are similar.

B. Temperature Effect on Brinell Hardness

Temperature effects on the Brinell hardness of SS 304, Ni 200 and Al 6061 T6 were found by Nho[20]. The load was 1500 kg and the ball diameter was 10 mm for the Brinell test on SS 304 and Ni 200. Five measurements of the indentation diameter were made at the reported temperatures. The average values for SS 304 are given in Table 7.

Table 7. Temperature effect on Brinell hardness of SS 304

T(°C)	d(mm)	H_B(MPa)	$H_B(T)/H_B(23.8)$
23.8	3.68	1335	1.00
55.6	3.79	1256	0.94
89.9	3.89	1189	0.89
123.0	4.00	1122	0.84
152.4	4.07	1082	0.81
186.1	4.15	1039	0.78

The correlation equation is

$$\frac{H_B(T)}{H_B(23.8)} = \exp\left[C_T\,(T - 23.8)\right] \tag{57}$$

where the correlation coefficient is $C_T = -1.51 \times 10^{-3}\,\mathrm{C}^{-1}$.

The average values for Ni 200 are given in Table 8.

Table 8. Temperature effect on Brinell hardness of Ni 200

T(°C)	d(mm)	H_B(MPa)	$H_B(T)/H_B(23.1)$
23.1	3.51	1472	1.00
58.5	3.62	1381	0.94
95.1	3.70	1320	0.90
121.8	3.80	1249	0.85
159.0	3.91	1177	0.80
209.3	4.17	1028	0.70

The correlation equation for Ni 200 is

$$\frac{H_B(T)}{H_B(23.1)} = \exp\left[C_T\,(T - 23.1)\right] \tag{58}$$

where the correlation coefficient is $C_T = -1.86 \times 10^{-3}\,\mathrm{C}^{-1}$.

For the temperature tests for Al 6061 T6 the load was 500 kg and the ball diameter was 10 mm. Five measurements of the indentation diameter were made at the reported temperatures. The average values for Al 6061 T6 are given in Table 9. The correlation equation is

Table 9. Temperature effect on Brinell hardness of Al 6061 T-6

T(°C)	d(mm)	H_B(MPa)	$H_B(T)/H_B(22.3)$
22.3	2.59	915	1.00
48.9	2.61	901	0.98
71.1	2.64	880	0.96
102.3	2.68	854	0.93
124.3	2.72	828	0.91
140.8	2.77	798	0.87
164.3	2.81	775	0.85
195.6	2.86	748	0.82

$$\frac{H_B(T)}{H_B(22.3)} = \exp\left[C_T\,(T - 22.3)\right] \tag{59}$$

where the correlation coefficient is $C_T = -1.20 \times 10^{-3}\,\mathrm{C}^{-1}$.

C. Temperature Effect on Vickers Microhardness and Correlation Coefficients

The hot Vickers microhardness tests and correlations are from Nho[20]. He conducted tests with Ni 200, SS 304, and Al 6061-T6. He obtained indentation data from three tests and reported the average values. Six loads were used: $(F = 25, 50, 100, 200, 300, 500)$ kg. Tests were conducted at room temperature and 4 higher temperature levels.

The Vickers microhardness results were correlated with the power-law relation:

$$H_V = c_1 \left(\frac{d_V}{d_0}\right)^{c_2} \qquad \text{with} \quad d_0 = 1\,\mu\text{m} \tag{60}$$

For the three metals tested the correlation coefficient $c_1(T)$ was dependent on the test temperature while the size index c_2 was independent of the temperature. For Ni 200 the values of c_2 lie in the narrow range of -0.209 to -0.237. The average value $c_2 = -0.226$ was selected and a new set of values for $c_1(T)$ were calculated.

For SS 304 the values of c_2 lie in the narrow range of -0.265 to -0.289. The average value $c_2 = -0.279$ was selected and a new set of values for $c_1(T)$ were calculated.

For Al 6061 T-6 the values of c_2 lie in the narrow range of -0.00643 to -0.0117. The average value $c_2 = -0.0079$ was selected and a new set of values for $c_1(T)$ were calculated.

The values of $c_1(T)$ for each metal were correlated and the following general relationship was given

$$\frac{c_1(T)}{c_1(T_{rm})} = \exp\left[C_T\,(T - T_{rm})\right] \qquad 25 \le T \le T_{max} \tag{61}$$

The correlation parameters $c_1(T_{rm})$, C_T, and T_{max} are given in Table 10. The room temperatures for the Vickers microhardness tests for Ni 200, SS 304, and Al 6061 T-6 were $T_{rm} = 22.9$, 25.2, 23.7°C, respectively.

For Ni 200 with $c_2 = -0.226$ the re-correlated values are listed in Table 11. For SS 304 with $c_2 = -0.279$ the re-correlated values are listed in Table 12. For Al 6061 T-6 with $c_2 = -0.0079$ the re-correlated values are listed in Table 13.

Table 10. Temperature coefficients for Brinell hardness of three metals

Metal	$c_1(T_{rm})$(MPa)	$10^3 C_T(\mathrm{C}^{-1})$	$T_{max}(^\circ\mathrm{C})$
Ni 200	6636	-1.372	186
SS 304	7339	-1.675	190
Al 6061 T-6	1123	-1.190	183

Table 11. Temperature effect on coefficients for Ni 200

T($^\circ$C)	c_1(MPa)	$c_1(T)/c_1(T_{rm})$	Max.%diff.
22.9	6636	1.00	+2.6
$48.4 - 45.9$	6282	0.95	-2.7
$95.6 - 82.3$	6115	0.92	-2.3
$156.5 - 138.0$	5613	0.85	-2.5
$185.9 - 179.7$	5258	0.79	-2.9

Table 12. Temperature effect on coefficients for SS 304

T($^\circ$C)	c_1(MPa)	$c_1(T)/c_1(T_{rm})$	Max.%diff.
25.2	7339	1.00	-1.5
$61.6 - 54.3$	6716	0.92	-2.7
$114.3 - 92.8$	6321	0.86	-2.9
$150.8 - 146.1$	5898	0.80	+2.3
$197.2 - 182.4$	5495	0.75	+2.7

Table 13. Temperature effect on coefficients for Al 6061 T-6

T($^\circ$C)	c_1(MPa)	$c_1(T)/c_1(T_{rm})$	Max.%diff.
23.7	1123	1.00	+1.8
$52.3 - 48.1$	1104	0.98	-1.8
$92.4 - 86.4$	1072	0.95	-1.4
$157.0 - 156.4$	1013	0.90	+1.8
$183.0 - 177.9$	909	0.81	-1.8

VII. Nano-Indentation Tests

A comprehensive review of nanoindentation tests and nanohardness is beyond the scope of this paper. Therefore, a relatively short review of the important features of nanoindentation tests will be presented. Details are available in the text[14] and in a few papers[24−27].

The indenter of choice is the Berkovich (three-sided) indenter, although the Vickers indenter has been used.

As the indenter is slowly forced into the surface of the specimen, both elastic and plastic deformation processes occur, and a contact area is produced that conforms to the shape of the indenter. The displacement h and the load P are continuously monitored until the maximum load P_{max} is reached and the corresponding penetration depth is h_{max}. As the indenter is slowly withdrawn, only the elastic portion of the displacement is recovered. The unloading load and displacement are continuously monitored until the load is zero and the final or residual penetration depth h_f measured. The loading and unloading curves are shown schematically in Fig. 9.

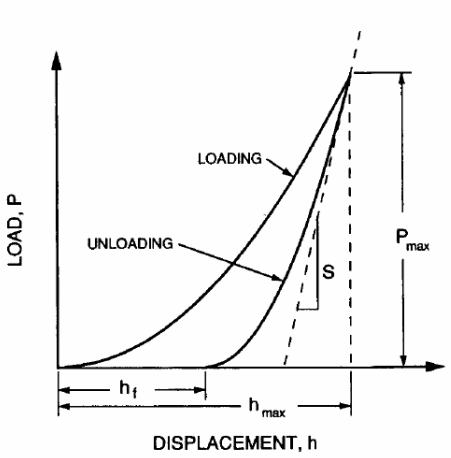

Figure 9. Typical Loading and Unloading Curves for Nanoindentation Tests. (From Oliver and Pharr, 1992).

The load range is typically from zero to $P_{max} = 200\,\text{mN}$ and the penetration depth is from zero to $h_{max} = 1000\,\text{nm}$. Figure 10 shows unloading nanoindentation curves for 6 different materials[25]. The horizontal axis is the relative displacement $(h - h_f)$ which shows clearly the different unloading trends. The Aluminum and Tungsten unloading curves are very similar.

The slope of the upper portion of the unloading curve is denoted as $S = dP/dh$ as shown in Fig. 11[24]. The parameter S is called the elastic contact stiffness[14,24−27]. The elastic modulus E and the nano or microhardness H are derived from these quantities by a set of relationships based on elasticity theory. Figure 11 also shows the contact penetration depth h_c for an ideal circular punch where $\epsilon = 1$, and the contact depth for the Berkovich indenter with $\epsilon = 0.72$.

The fundamental relationships from which H and E are determined are:

$$H = \frac{P}{A} \tag{62}$$

where P is the load and A is the *projected* contact area at that load, and

$$E_r = \frac{\sqrt{\pi}}{2\beta}\frac{S}{\sqrt{A}} \tag{63}$$

where E_r is the reduced elastic modulus of the contact and β is a constant that depends on the geometry of the indenter. The reduced modulus is defined as

$$\frac{1}{E_r} = \frac{1-\nu^2}{E} + \frac{1-\nu_i^2}{E_i} \tag{64}$$

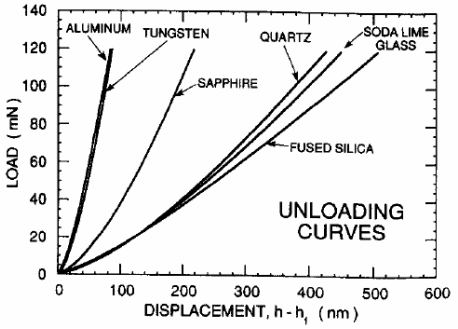

Figure 10. Final Unloading Curves Versus Reduced Displacements for Six Materials. (From Oliver and Pharr, 1992).

where E and ν are the elastic modulus and Poisson's ratio of the test specimen, and E_i and ν_i are the elastic modulus and Poisson's ratio of the indenter.

The reduced modulus is used to account for the fact that elastic displacements occur in the specimen and the indenter. For a diamond indenter the values $E_i = 1140\,\text{GPa}$ and $\nu_i = 0.07$ are frequently used.

The reduced modulus requires the Poisson's ratio of the specimen which is unknown. However, the value $\nu = 0.25$ produces a 5% uncertainty in the calculated value of E for most materials.

The equation for the reduced elastic modulus is based on the classical problem of the axisymmetric contact of a smooth, rigid, circular punch with an isotropic elastic halfspace whose elastic properties E and ν are constants. For this type of indenter the geometric parameter value is $\beta = 1$. However, it has been shown that the equation can be applied to indenters whose geometry is not axisymmetric, provided appropriate values of β are used. For indenters with square cross sections such as the Vickers pyramid, $\beta = 1.01$, and for the triangular cross section such as the Berkovich pyramid, $\beta = 1.034$.

In order to implement the method to calculate H and E accurately from the indentation load-displacement data, one must have an accurate measurement of the elastic contact stiffness S and the *projected* contact area A under the load P.

The widely used method of establishing the contact area was proposed by Oliver and Pharr[24] which expands on the ideas by others[14,25–27]. The first step of the analysis procedure consists in fitting the unloading part of the load-displacement data to the power-law relation derived from the elastic contact theory:

$$P = B(h - h_f)^m \tag{65}$$

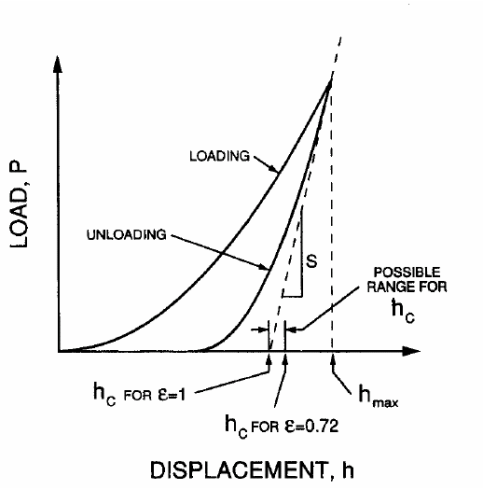

Figure 11. Schematic of Loading and Unloading Curves Versus Displacements Showing Quantities Used in Analysis. (From Oliver and Pharr, 1992) .

where B and m are empirically determined fitting parameters, and h_f is the final displacement after complete unloading. Its also determined from the curve fit.

The second step in the analysis consists of finding the contact stiffness S by differentiating the unloading curve fit, and evaluating the result at the maximum depth of penetration, $h = h_{max}$. This gives

$$S = \left(\frac{dP}{dh}\right)_{h=h_{max}} = Bm(h_{max} - h_f)^{m-1} \tag{66}$$

The third step in the procedure is to determine the contact depth h_c which for elastic contact is smaller than the total depth of penetration. The contact depth is estimated according to[24]

$$h_c = h_{max} - \epsilon \frac{P_{max}}{S} \tag{67}$$

where ϵ is another constant that depends on the indenter geometry. This geometric parameter has the value $\epsilon = 0.75$ for spherical indenters, and $\epsilon = 0.72$ for conical indenters. Experiments with Berkovich indenters (three-sided pyramidal indenters) have shown that $\epsilon = 0.75$ works well even when there is elastic-plastic deformation during unloading. It should be noted that the correction for h_c should be used with some caution because it is not valid in the case of material pile-up around an indent. Therefore inspection of the residual impression using a scanning electron microscope (SEM) or an atomic force microscope (AFM) is useful.

If we assume that the Berkovich indenter is ideal, then the relation

$$\left.\begin{aligned} A &= 3\sqrt{3}\,\tan^2 65.3^\circ\, h_c^2 \\ &= 24.5\, h_c^2 \end{aligned}\right\} \tag{68}$$

is valid, and fitting the upper 25% to 50% of the unloading curve is sufficient.

If the indenter tip is blunted or it has other defects, then the following procedure is recommended.

In the last step in the analysis the *projected* contact area is calculated by evaluating an empirically determined indenter area function $A = f(h)$ at the contact depth h_c such that

$$A = f(h_c) \tag{69}$$

The area function $A = f(h_c)$ is also called the shape function or tip function because it relates the cross-sectional area of the indenter A to the distance h_c from its tip.

A general polynomial form is used[24]

$$A = 24.5h_c^2 + \sum_{i=1}^{n} C_i \, h_c^{1/2^i} \tag{70}$$

The leading term of the polynomial fit corresponds to the ideal Berkovich indenter, and the remaining terms account for deviations from the ideal geometry due to indenter tip rounding. The number of terms is chosen to give a good fit over the entire range of depths as assessed by comparing a log-log plot of the fit with the data. Because the data are often obtained over more than one order of magnitude in depth, a weighted fitting procedure should be used to assure that data from all depths have equal importance. The fitting parameters C_i can be obtained by performing nanoindentation tests on materials with known elastic modulus.

The procedure described above is essentially the one used by many researchers to obtain values of the elastic modulus E and the nanohardness H of many different materials. It is also used to determine these important physical properties of thin films and thin films bonded to substrates. The procedure continues to be modified for different applications. The normalized unloading curves for the 6 materials are shown in Fig. 12[24]. The procedure given above was used to obtain H and E for 6 materials. The power-law fit correlation coefficients[24] are listed in Table 14.

Table 14. Parameter values for power-law fits of unloading curve

Material	B (mN/nm^m)	m
Aluminum	0.2650	1.38
Fused silica	0.0500	1.25
Quartz	0.0215	1.43
Sapphire	0.0435	1.47
Soda-lime glass	0.0279	1.37
Tungsten	0.141	1.51

The good agreement between the calculated values of the contact area and the correlation equation is shown in Fig. 13[24]. Results for 3 materials are listed below. The values were obtained digitizing the values given Tables 15-17. The values for the first load were observed to lie below the values for the second load. Therefore, the digitized values were normalized with the second load values to show the trends of the data as the load increases. The values of hardness and elastic modulus for all materials show a definite size effect.

VIII. Summary and Conclusions

A brief review of the contact, gap and joint conductances for joints formed by the mechanical contact of conforming rough surfaces was presented. It was shown that the contact and gap conductances are complex parameters which depend on the effective surface roughness of the joint, the thermal conductivities of the contacting asperities and the gas in the microgaps, and the relative mean plane separation which was shown to depend on the apparent contact pressure and the contact microhardness.

Table 15. Values of hardness and elastic modulus for Aluminum

F(mN)	H(GPa)	ratio	F(mN)	E(GPa)	ratio
0.504	0.271	0.886	0.504	77.7	0.970
1.50	0.306	1.000	1.53	80.1	1.000
4.53	0.295	0.964	4.62	74.7	0.933
13.5	0.258	0.843	14.0	72.1	0.900
41.0	0.231	0.755	40.7	71.9	0.898
119	0.202	0.661	118	70.9	0.885

After a review of macrohardness indenters (Brinell, Meyer and Rockwell B), microhardness indenters (Berkovich, Knoop and Vickers), and the nanoindenter (Berkovich), it was shown that the contact microhardness is a complex parameter which depends on the effective joint surface roughness, apparent contact pressure, and the Vickers microhardness correlation coefficients.

The Vickers correlation coefficients are closely related to the Brinell hardness, and correlation equations are given.

The physical properties such as yield strength, Brinell hardness and Vickers microhardness are shown to be dependent on temperature level. Correlation equations are given for the temperature effect.

A brief review of nanoindentation tests and procedures for calculating the elastic modulus and hardness was given, and some results from nanoindentation tests are given for several materials.

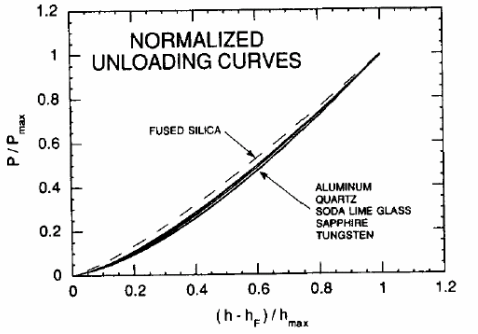

Figure 12. Normalized Final Unloading Curves Versus Displacements for Six Materials Showing Similar Trends. (From Oliver and Pharr, 1992).

Table 16. Values of hardness and elastic modulus for Tungsten

Load(mN)	Hardness(GPa)	Load(mN)	Modulus(GPa)
0.512	5.86	0.499	372.0
1.49	5.67	1.48	495.0
4.53	5.21	4.49	427.0
13.2	4.55	13.6	403.0
40.9	3.88	41.1	401.0
119	3.75	120	400.0

Table 17. Values of hardness and elastic modulus for Quartz

Load(mN)	Hardness(GPa)	Load(mN)	Modulus(GPa)
0.506	12.9	0.515	119.0
1.50	13.8	1.50	122.0
4.46	13.3	4.63	119.0
13.5	13.2	13.8	123.0
40.2	12.5	40.8	121.0
117	12.4	121	125.0

In general the contact microhardness is a complex parameter because it depends on the effective joint surface roughness, the apparent contact pressure, the bulk hardness, and the temperature level.

Acknowledgments

The author gratefully acknowledges the support of the Natural Sciences and Engineering Research Council of Canada (NSERC). The assistance of Dr. Waqar Khan in the preparation of this paper is greatly appreciated.

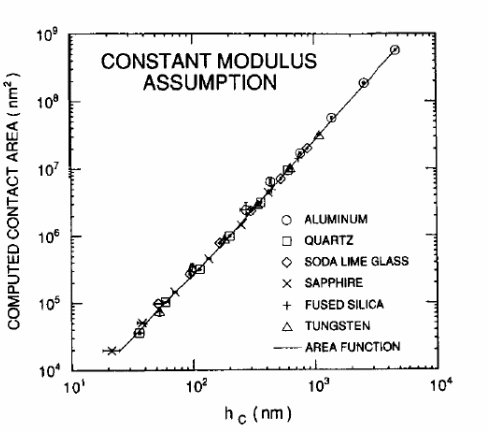

Figure 13. Calculated Contact Areas Versus Contact Depths for Six Materials. (From Oliver and Pharr, 1992).

References

[1] Yovanovich, M.M. and Marotta, E.E. (2003). Chapter 4, "Thermal Spreading and Contact Resistances," *Heat Transfer Handbook*, John Wiley & Sons, Editors: Adrian Bejan and Alan D. Kraus, New York, NY.

[2] Mantelli, M.B.H. and Yovanovich, M.M. (2002). Chapter 16 "Thermal Contact Resistance," *Spacecraft Thermal Control Handbook*, Volume I: Fundamental Technologies, Second Edition, Editor: David G. Gilmore, The Aerospace Press, El Segundo, CA.

[3]Cooper, M.G., Mikic, B.B., and Yovanovich, M.M. (1969). "Thermal Contact Conductance," *Int. J. Heat Mass Transfer*, Vol. 12, pp. 279-300.

[4]Yovanovich, M.M. (1981). "New Contact and Gap Conductance Correlations for Conforming Rough Surfaces," AIAA Paper No. 81-1164, AIAA 16th Thermophysics Conference, Palo Alto, CA, June 23-25. Published in AIAA Progress in Astronautics and Aeronautics, *Spacecraft Radiative Transfer and Temperature Control*, Vol. 83, pp. 83-95, 1982. Editor Dr. T.E. Horton.

[5]Yovanovich, M.M., DeVaal, J. and Hegazy, A. (1982). "A Statistical Model to Predict Thermal Gap Conductance Between Conforming Rough Surfaces," AIAA 82-0888, AIAA/ASME 3rd Joint Thermophysics, Fluids, Plasma and Heat Transfer Conference, St. Louis, MO, June 7-ll.

[6]Yovanovich, M.M., Hegazy, A.A., and DeVaal, J. (1982). "Surface Hardness Distribution Effects Upon Contact, Gap and Joint Conductances," AIAA 82-0887, AIAA/ASME 3rd Joint Thermophysics, Fluids, Plasma and Heat Transfer Conference, June 7-11, St. Louis, Missouri.

[7]Negus, K.J. and Yovanovich, M.M. (1988). "Correlation of Gap Conductance Integral for Conforming Rough Surfaces", *Journal of Thermophysics and Heat Transfer*, Vol. 2, No. X, pp. 279-281, March.

[8]Song, S. (1988). "Analytical and Experimental Study of Heat Transfer Through Gas Layers of Contact Interfaces," Ph.D. Thesis, University of Waterloo, Canada.

[9]Song, S. and Yovanovich, M.M. (1988). "Relative Contact Pressure: Dependence Upon Surface Roughness and Vickers Microhardness," *Journal of Thermophysics and Heat Transfer*, Vol. 2, No. 1, pp. 43-47, January.

[10]Mott, M.A. (1956). *Micro-Indentation Hardness Testing*, Butterworths Scientific Publications, London.

[11]Tabor, D. (1951). *Hardness of Metals*, Oxford University Press, London.

[12]Johnson, K.L. (1985). *Contact Mechanics*, Cambridge University Press, Cambridge.

[13]McColm, I.J. (1990). *Ceramic Hardness*, Plenum Press, New York, NY.

[14]Fisher-Cripps, A.C. (2000). *Introduction to Contact Mechanics*, Springer, New York, NY.

[15]Yovanovich, M.M., Hegazy, A.A., and DeVaal, J. (1982). "Surface Hardness Distribution Effects Upon Contact, Gap and Joint Conductances," AIAA 82-0887, AIAA/ASME 3rd Joint Thermophysics, Fluids, Plasma and Heat Transfer Conference, June 7-11, St. Louis, Missouri.

[16]Yovanovich, M.M. and Hegazy, A. (1983). "An Accurate Universal Contact Conductance Correlation for Conforming Rough Surfaces with Different Micro-Hardness Profiles," AIAA 83-1434, AIAA 18th Thermophysics Conference, Montreal, Quebec, June 1-3.

[17]Yovanovich, M.M., Hegazy, A., and Antonetti, V.W. (1983). "Experimental Verification of Contact Conductance Models Based Upon Distributed Surface Micro-Hardness," AIAA-83-0532, AIAA 21st Aerospace Sciences Meeting, Reno, NV, January 1-13.

[18]Antonetti, V.W. (1983). "On the Use of Metallic Coatings to Enhance Thermal Contact Conductance," Ph.D. Thesis, University of Waterloo, Canada.

[19]Hegazy, A.A. (1985). "Thermal Joint Conductance of Conforming Rough Surfaces: Effect of Surface Microhardness Variation," Ph.D. Thesis, University of Waterloo, Canada.

[20]Nho, K.M. (1990). "Experimental Investigation of Heat Flow Rate and Directional Effect on Contact Conductance pf Anisotropic Ground/Lapped Interfaces," Ph.D. Thesis, University of Waterloo, Canada.

[21]Sridhar, (1994). "Elastoplastic Contact Models for Sphere-Flat and Conforming Rough Surface Applications," Ph.D. Thesis, University of Waterloo, Canada.

[22]Sridhar, M.R. and Yovanovich, M. M. (1994). "Review of Elastic and Plastic Contact Conductance Models: Comparison with Experiment," *Journal of Thermophysics and Heat Transfer*, Vol. 8, No. 4, Oct.-Dec., pp. 633-640.

[23]Sridhar, M.R. and Yovanovich, M. M., (1996). "Empirical Methods to Predict Vickers Microhardness," *Wear*, Vol. 193, pp. 91-98.

[24]Oliver, W.C. and Pharr, G.M. (1992). "An Improved Technique for Determining Hardness and Elastic Modulus Using Load and Displacement Sensing Indentation Experiments," *Journal of Materials Research*, Vol. 7, No. 6, pp. 1564-1583.

[25]Pharr, G.M., Oliver, W.C., and Brotzen, F.R. (1992). "On the Generality of the Relationship Among Contact Stiffness, Contact Area, and Elastic Modulus During Indentation," *Journal of Materials Research*, Vol. 7, No. 3, pp. 613-617.

[26]Hendrix, B.C. (1995). "The Use of Shape Correction Factors for Elastic Indentation Measurements," *Journal of Materials Research*, Vol. 10, No. 2, pp. 255-257.

[27]Hay, J.L. and Pharr, G.M. (2000). "Instrumented Indentation Testing," ASM Handbook Volume 08: Mechanical Testing and Evaluation, pp. 231-242. ASM International Materials Park, Ohio.